[Tectonics]

Supporting Information for

[Perspectives on continental rifting processes from spatiotemporal patterns of faulting and magmatism in the Rio Grande rift, USA]

[Alyssa L. Abbey[1,2,3], Nathan A. Niemi[1]]

[[1]Department of Earth and Environmental Sciences, University of Michigan, Ann Arbor, MI USA

[2]Now at Department of Earth and Planetary Science, University of California, Berkeley, CA, USA

[3]Now at Berkeley Geochronology Center, 2455 Ridge Road, Berkeley, CA, USA]

SUPPLEMENTARY INFORMATION, DATA TABLES, AND FIGURES

This document contains details on methods used for thermochronometric analysis and inverse thermal modeling and our volcanic data compilation, two data tables, Tables S1 and S2, and three supplementary figures, Figs. S1 – S3. Abbey and Niemi, 2018 contains examples of data files for inverse thermal history modeling, those files can be generated in the program QTQt with the information from Tables S1, S2 and data from the previously published data incorporated into each model run (Table 3). Alternatively, A.L. Abbey is willing to share the input text files used for these model runs and may be contacted at alabbey@berkeley.edu.

Table S1: This table contains analytical data for all apatite and zircon grains used for apatite (U-Th-Sm)/He and zircon (U-Th)/He thermochronometry results presented in this manuscript.

Table S2: This table contains information about input parameters used in the thermal history modeling with QTQt.

Figure S1: This figure shows relationships between age and eU and age and grain size.

Figure S2: This figure shows relationships between the observed age the predicted age from the maximum likelihood model output from QTQt.

Figure S3: This figure shows relationships between major oxides (SiO_2, Na_2O, and K_2O wt%) within the different Cenozoic volcanic fields in New Mexico and Colorado.

Low-temperature thermochronometry analyses

Here we primarily compile published low-temperature thermochronometry data and then complement these data with new thermochronometric analyses that expand the temperature ranges of the existing data. For our new samples we analyzed 4-5 crystals per AHe sample and three crystals per ZHe sample. Outliers in each of the samples were identified using Dean and Dixon's q-test (Dean and Dixon, 1951; Abbey et al., 2017) and individual crystals were excluded if they were considered outliers with 95% confidence (Table S1). Sample age results are highly reproducible with percent errors of <8% after removal of outliers (Table 3).

Inverse thermal history modeling parameters

Inverse thermal history modeling of low-temperature thermochronometric data in QTQt (Gallagher, 2012) includes three main parts: (1) the thermochronometric data, (2) any additional geologic information, and (3) system- and model-parameters (Table S2). Inverse thermal model inputs include raw age information, grain size, and concentrations of He, U, Th and Sm. In all model runs we implemented the Flowers et al. (2009) model for radiation damage in apatite (RDAAM) and the Guenthner et al. (2013) damage model for zircon (ZrDAAM) (Table S2). Our defined model parameters include present-day surface temperatures between 7°C and 13°C (temperatures that encompass the mean annual temperatures in the rift basins in Colorado and New Mexico), and a geothermal gradient between 25°C and 35°C/km (30°C/km is a reasonable estimate for the RGR based on modern regional heat flow as well as elevated heat flow estimates for the region during the Oligocene; House et al., 2003). The prior temperature range for each model (i.e. the temperature space in which a single model run can start) was dependent on the types of data included in the runs (with AHe data alone the temperature prior was set to between 0°C and 100°C, if AFT data was included the temperature priors were between 0°C and 150°C, and if ZHe was included the temperature prior was between 0°C and 250°C) (Table S2). In select cases, other useful published information related to past temperatures or depths was incorporated into the models as a constraint. Such the individual constraints are discussed below (Figs. 4 and 5). Models were run with a burn-in of 20,000 iterations then sampled over 100,000 iterations and the birth proposal parameters were picked using a Gaussian distribution (Table S2). Model prediction fits are available in the supplementary information (Fig. S2). In addition, newer versions (post-QTQt64R5.5) of the program are helpful for including early AFT data published in the region, because these early publications often omitted the detailed track count and track length data needed for inverse modeling to obtain thermal histories. More recent versions of QTQt provide an option to simulate populations of spontaneous and induced track length data with statistical distributions that match those of the original data (for which summary statistics and not full distributions are commonly provided), thus allowing the incorporation of earlier AFT data into modern thermal history models.

Volcanic data compilation and filtering

We compiled chemical and age data related to all volcanic rocks in NM and CO with ages from 70 to 0 Ma from EarthChem; http://www.earthchem.org/portal, accessed February 2018. We note that although every reported sample had an age associated with it, not every study performed independent age dating, such that many of the reported ages were assigned through regional correlations or stratigraphic relationships. We accept this method for assigning ages and use these data in our assessment of spatial and temporal patterns of magmatism. To ensure

accurate oxide weight percent (wt%) values we retained only samples with total major oxide concentrations between 98% and 102% (n = 5064) to use in our assessment (Figs. 6 and 7). We did not filter the data to show one point per volcanic flow event; however, Chapin et al. (2004) perform a similar compilation for Cenozoic magmatic rocks in New Mexico from a database compiled by the New Mexico Bureau of Geology and Mineral Resources (Wilks and Chapin, 1997; database updated and maintained by Maureen Wilks from 1997 until at least 2004). The compilation by Chapin et al. (2004) filters the data so that there is only one point per erupted event or specific stratigraphic horizon. The trends in their compilation for NM volcanic rock data are similar to ours gathered for both NM and CO, thus we do not believe that there is a large bias introduced by not further filtering the results from our EarthChem query (Table 4).

TABLE S1. INDIVIDUAL GRAIN RESULTS FOR APATITE AND ZIRCON HE SAMPLES

Sample Name & Mineral (A or Z)	Mass (µg)	Length (µm)	Radius (µm)	FT	U (ppm)	Th (ppm)	Sm (ppm)	He (ncc)	eU (ppm)	Raw date (Ma)	Corr. date (Ma)	Error (Ma)
17NSdCb (A)	4.04	156.8	56.5	0.79	28.05	35,57	419.19	0.11	37.9	6.1	7.76	0.07
17NSdCd (A)	6.54	173.1	68.5	0.82	1.71	5.28	32.73	0.02	3.1	5.4	6.63	0.08
17NSdCg (A)	1.99	146.2	41.1	0.72	19.92	36.03	501.63	0.05	30.7	6.3	8.75	0.07
17NSdCh (A)	2.32	121.9	48.6	0.75	15.55	30.24	292.77	0.03	24.0	4.9	6.49	0.06
17SDa (Z)	2.25	114.4	49.5	0.75	3897.93	55.37	--	16.00	3910.9	15.0	20.03	0.23
17SDb (Z)	4.83	174.9	58.5	0.79	196.76	108.21	--	1.94	222.1	14.9	18.80	0.20
17SDc (Z)	2.34	144.4	44.8	0.74	411.42	255.22	--	1.89	471.1	14.2	19.22	0.19
17WEELa (A)	2.39	114.0	51.0	0.76	14.98	6.33	50.23	0.03	16.7	6.1	8.00	0.09
17WEELb (A)*	3.68	129.4	59.4	0.79	19.48	3.58	40.21	0.15	20.5	16.4	20.83	0.23
17WEELc (A)	2.76	155.0	47.0	0.75	20.25	4.75	39.82	0.05	21.5	6.5	8.71	0.09
17WEELd (A)	4.81	121.9	70.0	0.81	16.67	3.17	30.56	0.07	17.6	6.6	8.16	0.09
17WEELe (A)	2.15	151.9	42.0	0.72	53.11	6.59	61.56	0.11	54.9	7.5	10.30	0.10
17SFea (A)	1.55	109.5	42.0	0.71	11.93	6.60	122.85	0.08	14.1	32.3	45.30	0.44
17SFeb (A)	1.02	249.6	71.3	0.83	40.01	1.66	269.97	2.78	41.7	55.0	66.01	0.78
17SFec (A)	2.81	137.4	50.4	0.76	17.87	3.92	148.89	0.29	19.5	44.6	58.65	0.66
17SFed (A)	5.00	181.1	58.5	0.80	20.01	2.27	220.27	0.60	21.8	47.3	59.41	0.67
17SFee (A)	6.17	222.2	58.7	0.80	13.78	1.98	119.62	0.55	14.8	51.2	63.92	0.79
17NBa (Z)	3.44	219.2	44.2	0.74	722.54	506.39	--	4.09	841.0	11.7	15.66	0.16
17NBb (Z)	3.01	162.5	47.9	0.75	874.10	430.11	--	3.66	974.7	10.3	13.68	0.14
17NBc (Z)	4.06	198.8	50.4	0.77	596.02	384.66	--	3.63	686.0	10.8	13.98	0.14

* Failed Q-Test for outliers, not used in mean age calculation or any other data analysis or interpretations.

S2. THERMAL HISTORY MODEL INPUT TABLE

Thermochronometric Data

Apatite (U-Th-Sm)/He or Zircon (U-Th)/He data: uncorrected age, error, concentrations of U, Th, Sm and He, mineral type, crystal size (length, width, height)

Apatite fission track data: all AFT data was from previously published studies, where those studies provided track count or track length data this was used, where those studies did not report the count or length data we used the resample count data function in QTQt to generate plausible track count data for the reported AFT age.

Additional Geologic Information

Most models were run without imposed constraint boxes. However, in places where there were concrete constraints on burial depths or surface exposure we did place large constrain boxes into the models with information on a range of temperatures that may have occurred over a range of times (e.g. 100 ± 50°C at 40 ± 10 Ma makes a box from 50 to 150°C and from 50 to 30 Ma).

System- and Model-specific Parameters

For each model run we had QTQt resample the errors associated with each grain age.

Both apatite and zircon grains were modeled as if they were spherical crystals because the ratios between grain length, width and height did not warrant a cylindrical model which is more complex and time consuming to run.

For apatite grains the RDAAM radiation damage model from Flowers et al., 2009 was used and for zircon the ZrDAAM radiation damage model from Guenthner et al., 2013 was used.

In this study the prior temperature ranges were adjusted to have a larger range (see section entitled Thermal modeling results and interpretation).

We used a 30°C/km geothermal gradient for all of our models, however we allowed the geothermal gradient to vary by 5°C so between 25°C and 35°C.

For present-day temperatures we used 10 ± 3°C (to account for the ranges in mean annual temperature for locations in CO and NM).

The present-day temperature offset was set to 6 ± 1°C/km as this is the accepted general topographic temperature effect at the surface.

The MCMC constraints we modified included the burn-in and post-burn-in values as well as the birth proposal parameters. We used 20,000 burn-in iterations, 80,000 post-burn-in iterations and a Gaussian birth proposal.

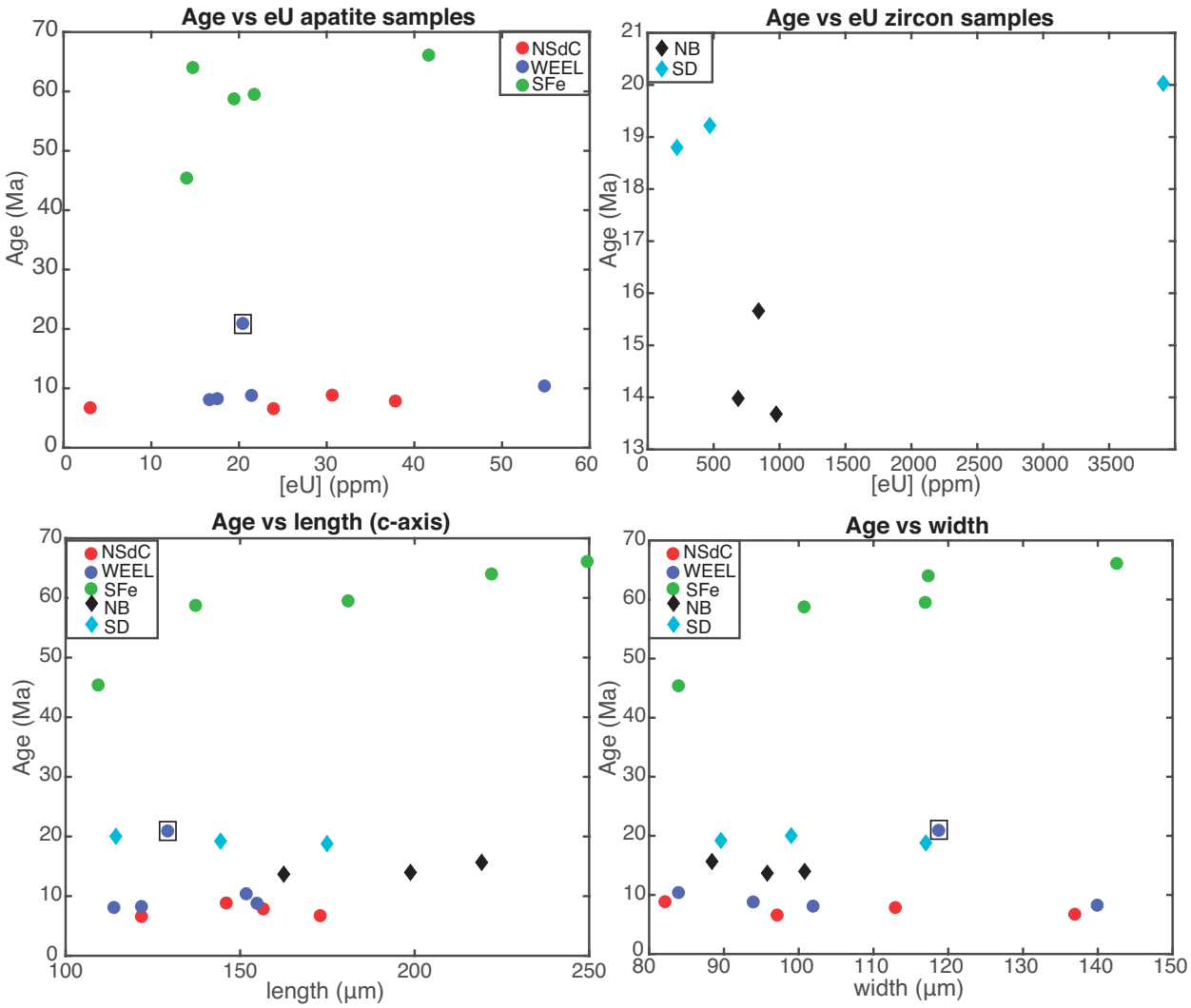

Figure S1. Plots of age-eU relationships for new thermochronometry data. Top panel: apatite grains—filled circles (left), zircon grains—filled diamonds (right). Bottom panel: age and grain size relationships (length and width, left and right respectively) for both apatite and zircon crystals (circles and diamonds respectively). Note one of the WEEL samples failed the q-test for outliers (blue circle with black box).

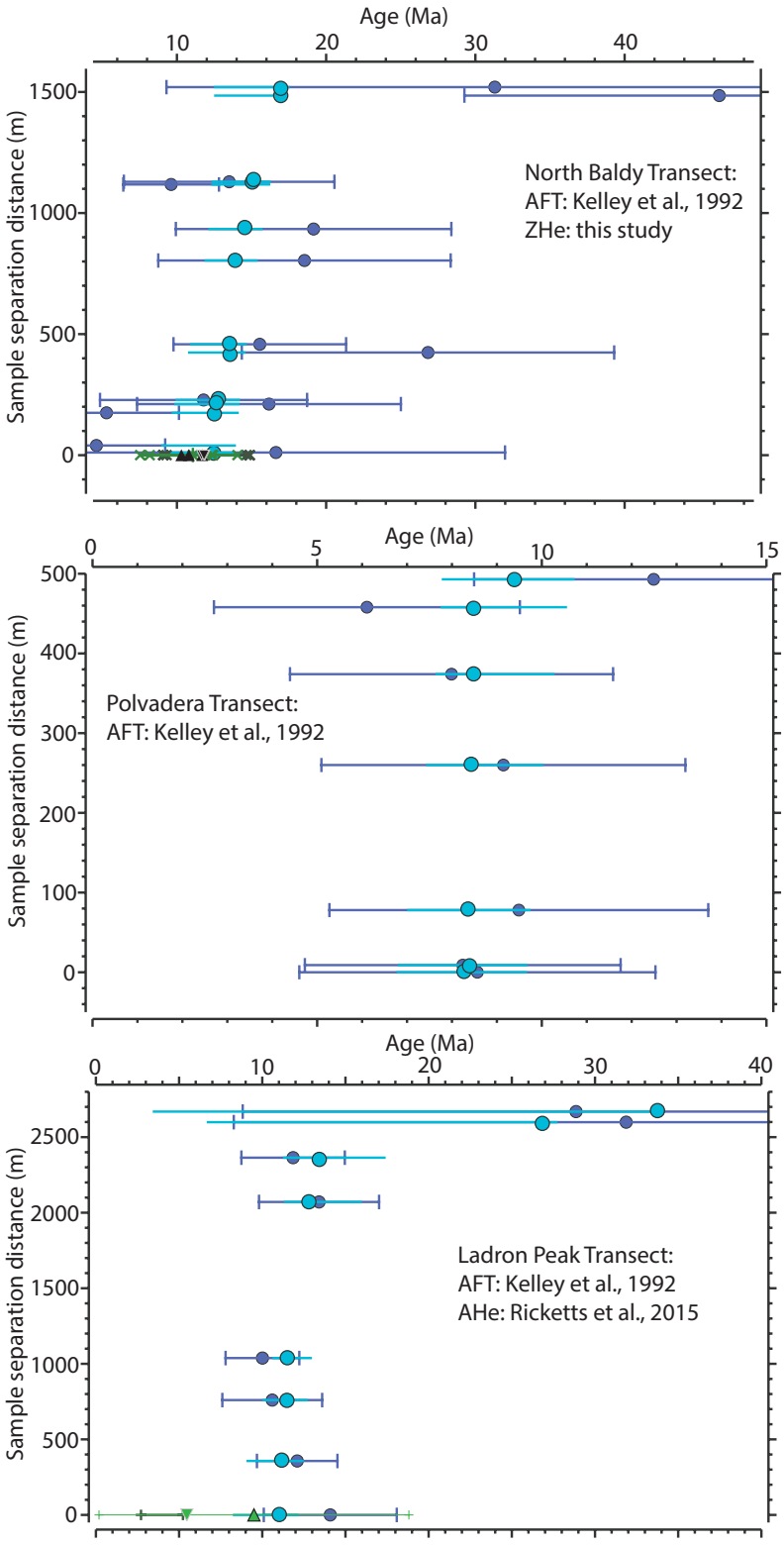

Figure S2 continued. AFT—apatite fission track; AHe—apatite (U-Th-Sm)/He; ZHe—zircon (U-Th)/He. This figure presents results from transects going south to north in the RGR. The above plots are all from the southern Albuquerque basin.

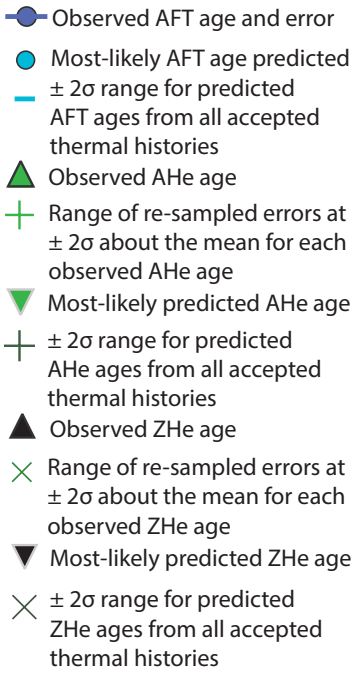

Figure S2. Plots of age versus sample separation distance for low-temperature thermochronometry data, both measured ages and predicted ages for the maximum likelihood model from QTQt thermal history runs for each transect (preferred thermal histories shown in Figs. 3.4, 3.5, and 3.6). Each plot is labeled with transect name, data type, and data source included in the inversion. For many of the AHe and ZHe analyses there were several grains analyzed from each sample, although these grains are all associated with one sample and that sample's respective elevation, QTQt splits individual grain results in vertical space (e.g. ZHe and AHe data in Sand Dunes transect). This does not mean the grains are representing different sample separation distance. Note, axes values are not the same for each plot.

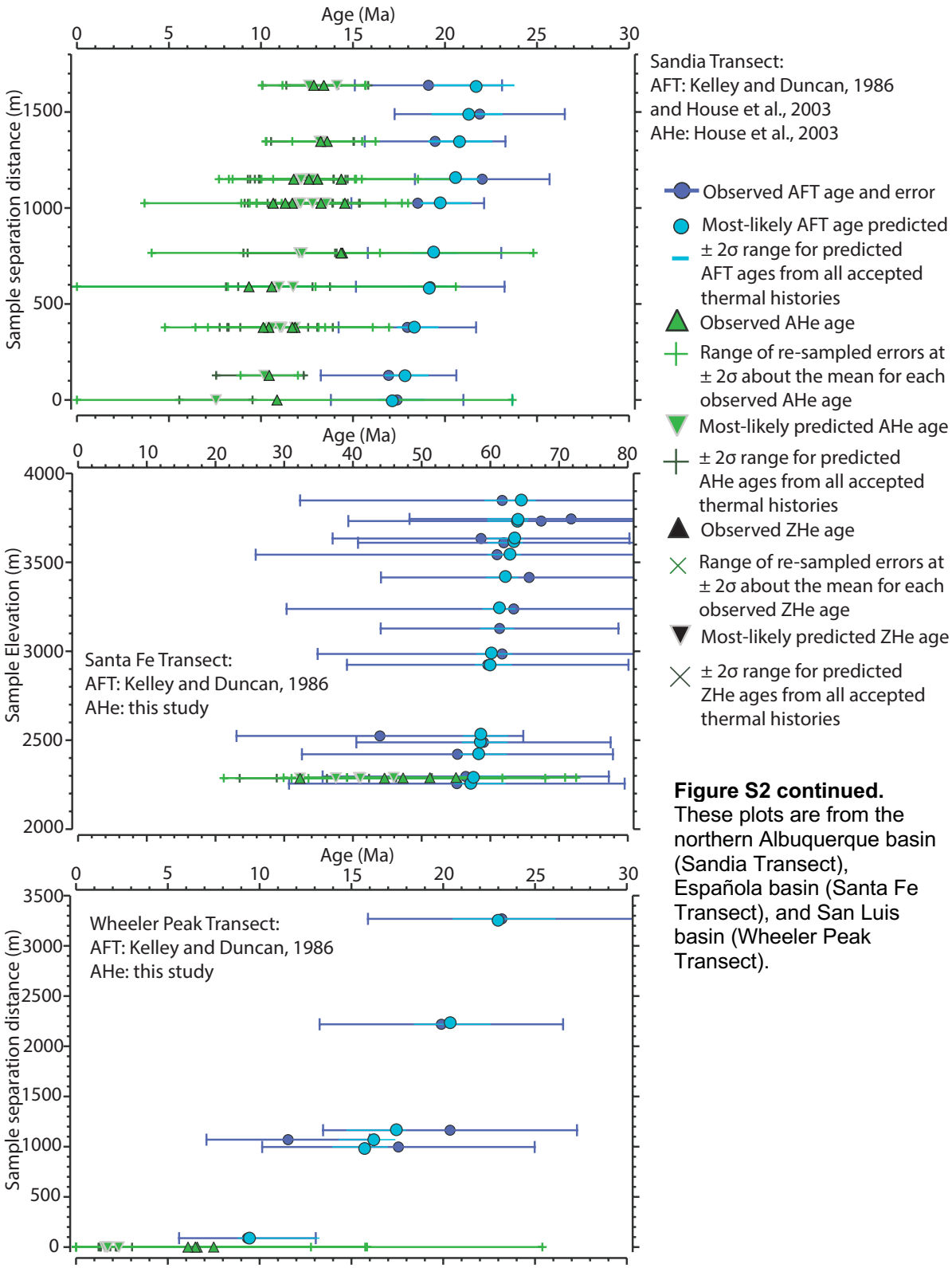

Figure S2 continued. These plots are from the northern Albuquerque basin (Sandia Transect), Española basin (Santa Fe Transect), and San Luis basin (Wheeler Peak Transect).

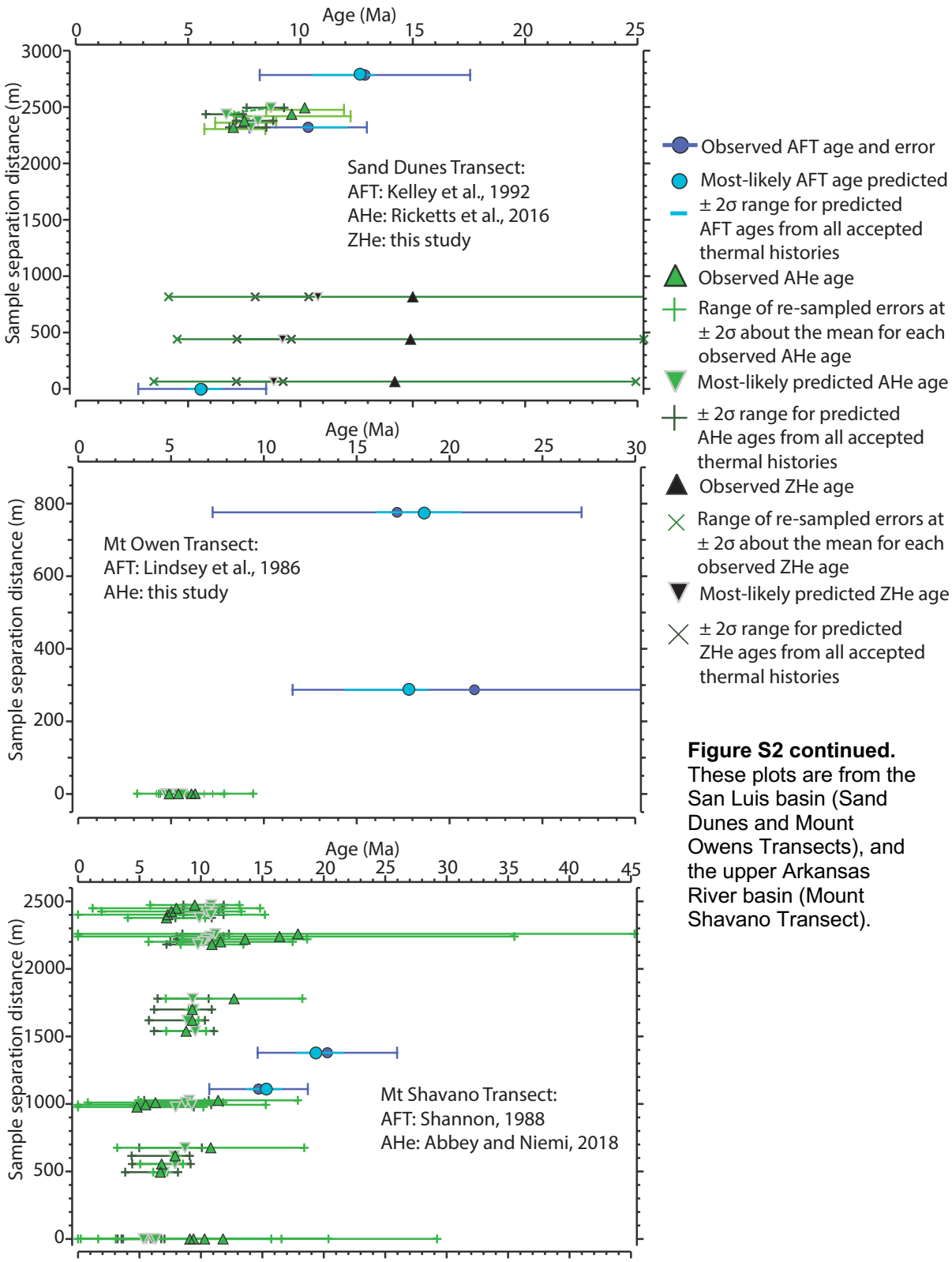

Figure S2 continued. These plots are from the San Luis basin (Sand Dunes and Mount Owens Transects), and the upper Arkansas River basin (Mount Shavano Transect).

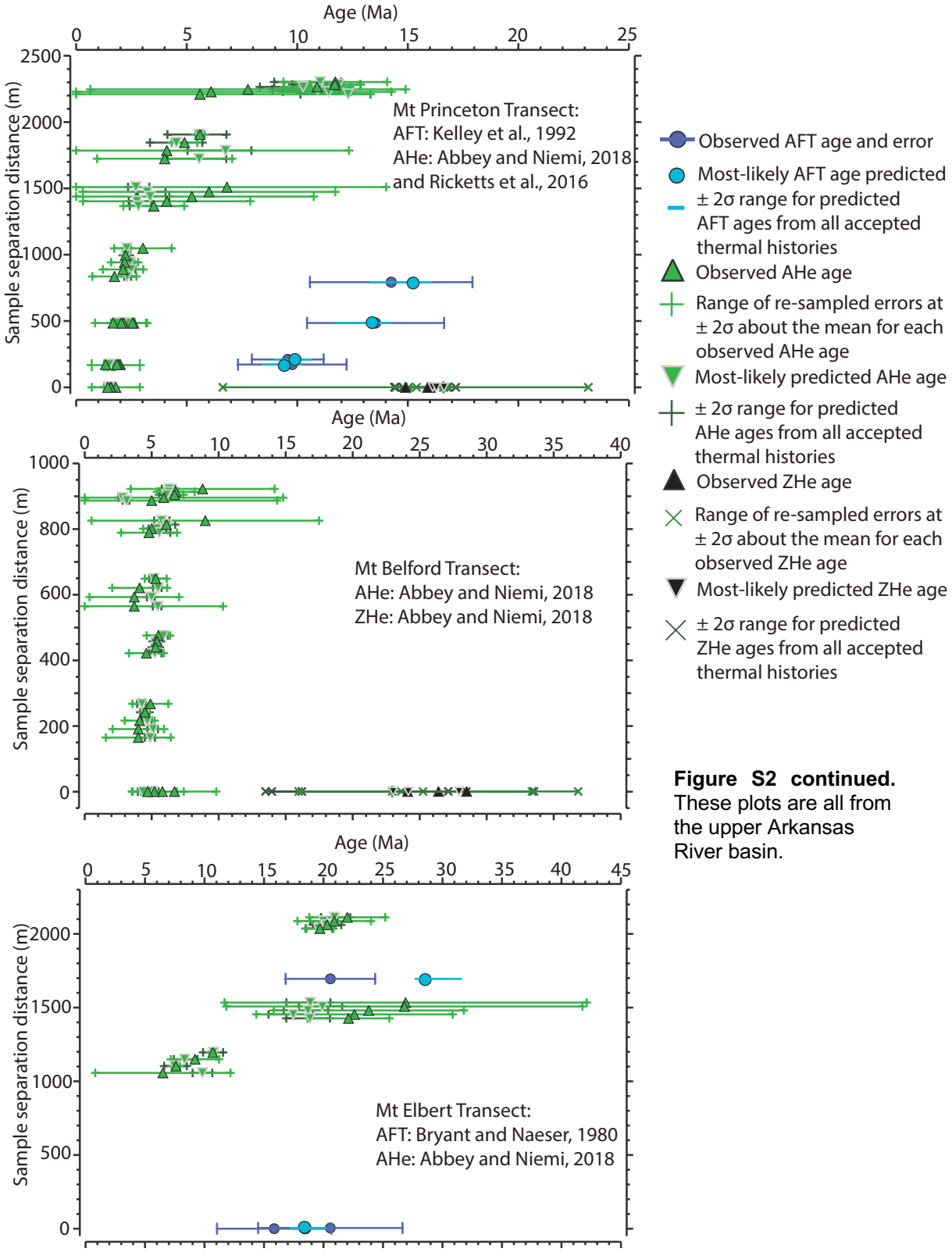

Figure S2 continued. These plots are all from the upper Arkansas River basin.

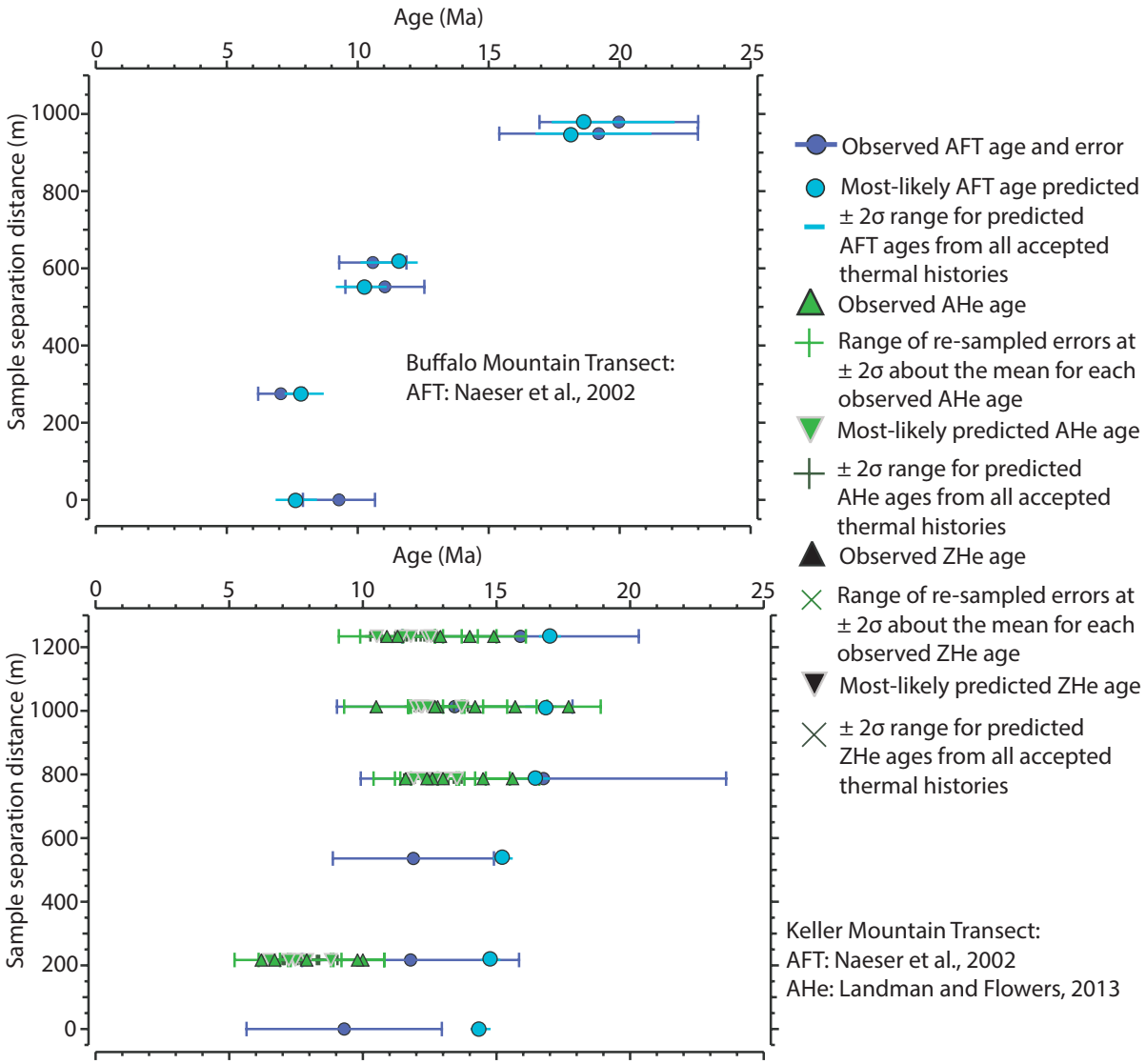

Figure S2 continued. The above plots are both from the Blue River basin

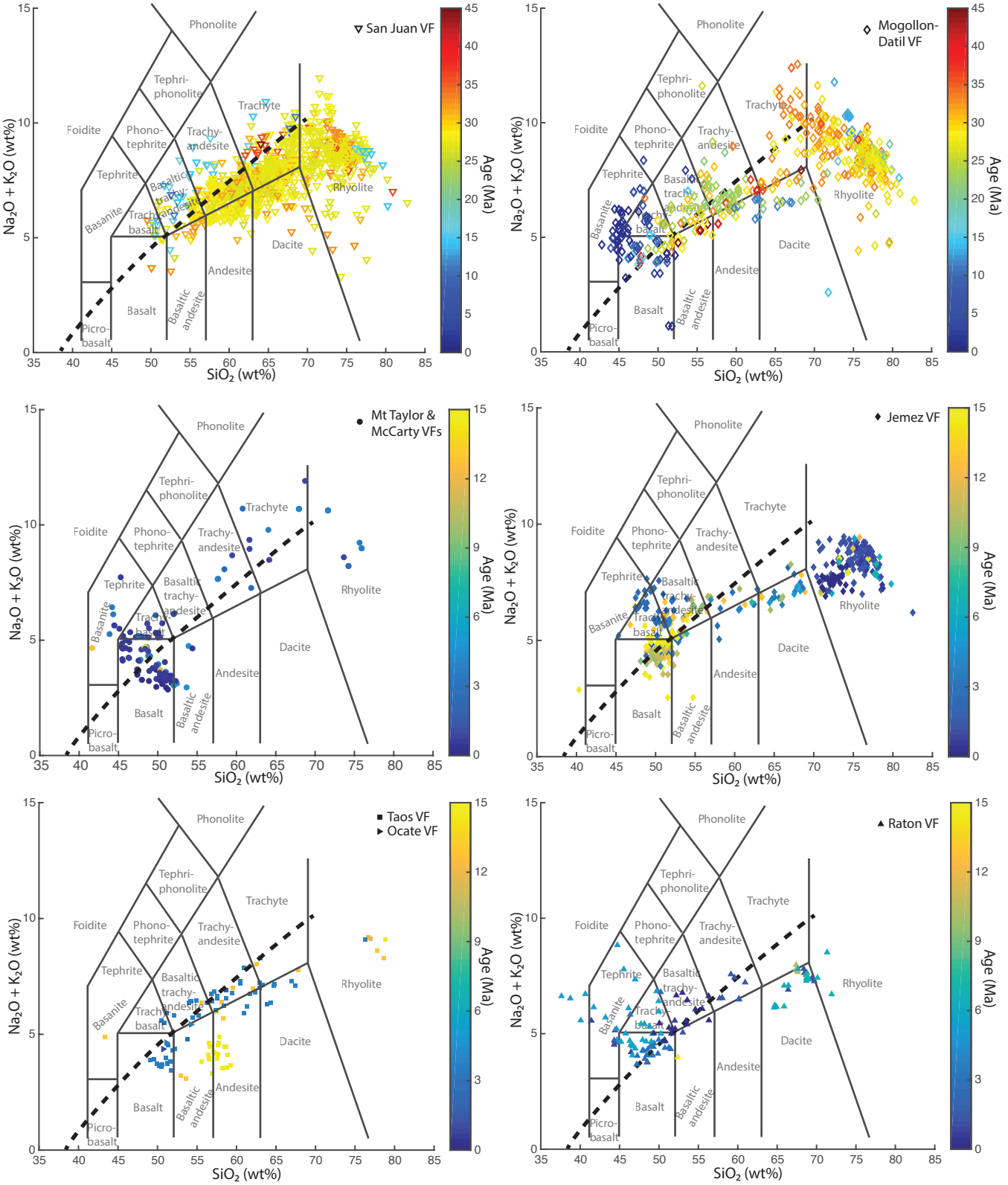

Figure S3: Plot of relationships between SiO2 and Na2O, and K2O data for each of the Cenozoic volcanic fields compiled in this study (Fig. 7; Table 4). Data is colored by age with each plot representing data from one volcanic field with the exception of two plots in the lower left corner, which show data from two volcanic field together. Bold dashed line separates alkaline compositions (top left side of line) from subalkaline and tholeitic compositions (bottom right side of line). Note that the ages represented in the top two plots are from 45 to 0 Ma and all the other plots show data from 15 to 0 Ma (no data for volcanic rocks older than 15 Ma in those fields). Volcanic fields include: San Juan, Mogollon-Datil, McCarty, Mount Taylor, Jemez, Taos, Ocate, and Raton.

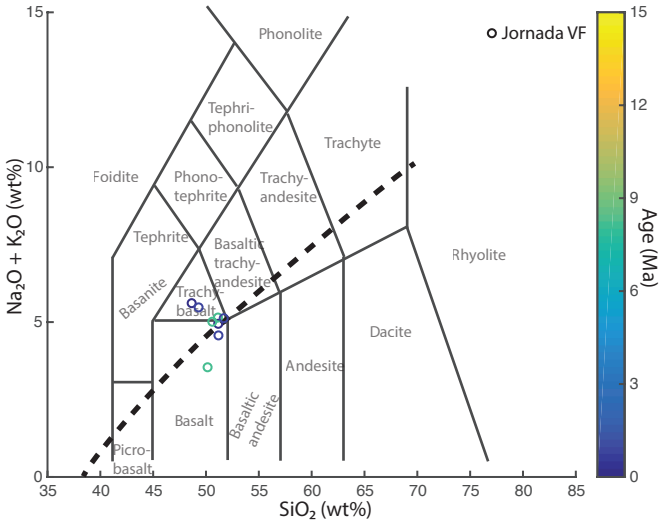

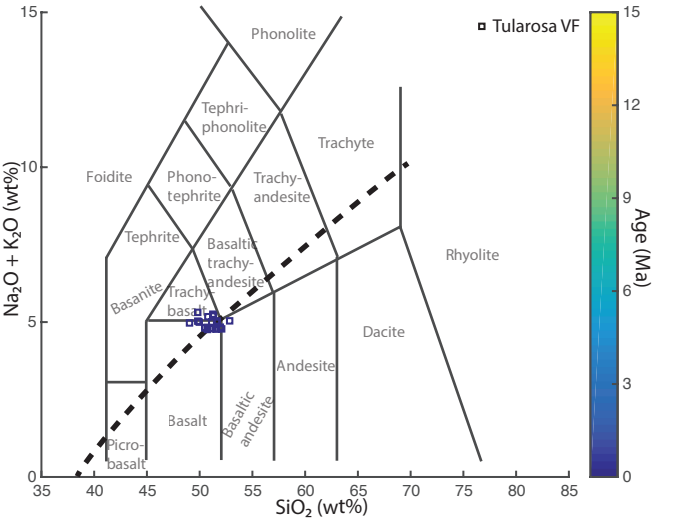

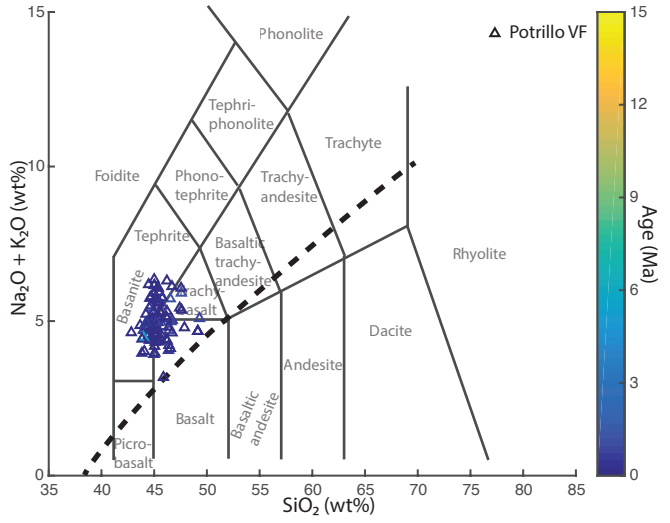

Figure S3 continued: Plots show data from 15 to 0 Ma (no data for volcanic rocks older than 15 Ma in these fields). Volcanic fields include: Jornada, Tularosa, and Potrillo.

REFERENCES

Abbey, A. L., & Niemi, N. A. (2018). Low-temperature thermochronometric constraints on fault initiation and growth in the northern Rio Grande rift, upper Arkansas River valley, Colorado, USA. *Geology, 46*(7), 627-630. doi:10.1130/G40232.1

Abbey, A. L., Niemi, N. A., Geissman, J. W., Winkelstern, I. Z., & Heizler, M. (2017). Early Cenozoic exhumation and paleotopography in the Arkansas River valley, southern Rocky Mountains, Colorado. *Lithosphere, 10*(2), 239-266. doi:10.1130/L673.1

Bryant, B., & Naeser, C. W. (1980). The significance of fission-track ages of apatite in relation to the tectonic history of the Front and Sawatch Ranges, Colorado. *Geological Society of America Bulletin, 91*, 156–164.

Chapin, C. E., Wilks, M., & McIntosh, W. C. (2004). Space-time patterns of late Cretaceous to present magmatism in New Mexico-comparison with Andean volcanism and potential for future volcanism. In Cather, S. M., McIntosh, W. C., & Kelley, S. A. (Eds.). *Tectonics, geochronology, and volcanism in the southern Rocky Mountains and Rio Grande rift* (Vol. 160, pp. 13–40). Socorro, New Mexico: Bureau of Geology and Mineral Resources Bulletin.

Dean, R. B., & Dixon, W. J. (1951). Simplified Statistics for Small Numbers of Observations. *Analytical Chemistry, 23*(4), 636–638.

Flowers, R. M., Ketcham, R. A., Shuster, D. L., & Farley, K. A. (2009). Apatite (U–Th)/He thermochronometry using a radiation damage accumulation and annealing model. *Geochimica et Cosmochimica Acta, 73*(8), 2347–2365.

Gallagher, K. (2012). Transdimensional inverse thermal history modeling for quantitative thermochronology. *Journal of Geophysical Research, 117*(B2).

Guenthner, W. R., Reiners, P. W., Ketcham, R. A., Nasdala, L., & Giester, G. (2013). Helium diffusion in natural zircon: Radiation damage, anisotropy, and the interpretation of zircon (U-Th)/He thermochronology. *American Journal of Science, 313*(3), 145-198.

House, M. A., Kelley, S. A., & Roy, M. (2003). Refining the footwall cooling history of a rift flank uplift, Rio Grande rift, New Mexico. *Tectonics, 22*(5), 1060.

Kelley, S. A., Chapin, C. E., & Corrigan, A. J. (1992). Late Mesozoic to Cenozoic Cooling Histories of the Flank of the Northern and Central Rio Grande Rift, Colorado and New Mexico. *New Mexico Bureau of Mines Mineral Resources, 145*, 1–40.

Kelley, S. A., & Duncan, I. J. (1986). Late Cretaceous to Middle Tertiary tectonic history of the northern Rio Grande rift, New Mexico. *Journal of Geophysical Research, 91*, 6246-6262.

Landman, R., & Flowers, R. M. (2013). (U-Th)/He thermochronologic constraints on the evolution of the northern Rio Grande Rift, Gore Range, Colorado, and implications for rift propagation models. *Geosphere, 9*(1), 170–187.

Lindsey, D. A., Andriessen, P. A. M., & Wardlaw, B. R. (1986). Heating, cooling, and uplift during Tertiary time, northern Sangre de Cristo Range, Colorado. *Geological Society of America Bulletin, 97*, 1133-1143.

Naeser, C. W., Bryant, B., Kunk, M. J., Kellogg, K., Donelick, R. A., & Perry, W. J. Jr. (2002). Tertiary cooling and tectonic history of the White River uplift, Gore Range, and western Front Range, central Colorado: Evidence from fission-track and $^{39}Ar/^{40}Ar$ ages. *Geological Society of America Special Papers, 366*, 31-53.

Ricketts, J. W., Karlstrom, K. E., & Kelley, S. A. (2015). Embryonic core complexes in narrow continental rifts: The importance of low-angle normal faults in the Rio Grande rift of central New Mexico. *Geosphere, 11*(2), 425-444.

Ricketts, J. W., Kelley, S. A., Karlstrom, K. E., Schmandt, B., Donahue, M. S., & van Wijk, J. (2016). Synchronous opening of the Rio Grande rift along its entire length at 25–10 Ma supported by apatite (U-Th)/He and fission-track thermochronology, and evaluation of possible driving mechanisms. *Geological Society of America Bulletin, v. 128*(3-4), 397–424.

Shannon, J. R. (1988). Geology of the Mount Aetna cauldron complex, Sawatch Range, Colorado. [Doctoral Thesis], Colorado School of Mines, Golden, CO.

Wilks, M., and Chapin, C. E., 1997, The New Mexico geochronological database: New Mexico Bureau of Mines and Mineral Resources, Digital Database Series, Database DDS–DB1, CDROM.